International Journal of Concrete Structures and Materials

RESEARCH

Open Access

Proposal for Bond Strength Considering Bond Characteristics of Beam Flexural Rebar on Interior Beam-Column Joints. Part II: Focusing on Column Axial Load, Beam Flexural Rebar Yield Strength and Diameter

Min-Su Jo[1], Hyeong-Gook Kim[2], Dong-Hwan Kim[1], Su-A Lim[1], Si-Hyeon Jeong[1], Jung-Yoon Lee[3] and Kil-Hee Kim[4*]

Abstract

To ensure the stability of interior beam-column joints under seismic loads, various influencing factors are incorporated into current design criteria in different countries. However, the design concepts and the influencing factors reflected in each country are different. The bond characteristics of beam longitudinal rebar penetrated the joint are mainly influenced by the compressive strength of concrete and are presented in the form of average bond stress. In Part I, the effect of concrete compressive strength on the bond characteristics of beam longitudinal rebar was directly investigated through a bond test that directly simulated the stress state of the joint. In this study, factors affecting the bond strength and required column depth were proposed by considering the bond characteristics based on the column axial force ratio and the yield strength of the beam longitudinal rebar. The experiment involved producing 14 test specimens and performing cyclic loading, taking each variable into consideration. Based on the experimental results, the proposed equation for the effect of column axial force ratio on the bond strength showed an excellent prediction performance compared to the current design equation with a coefficient of variation of 30.7%. In addition, a bond stress equation that reflects the stress difference of the beam longitudinal rebar was proposed using the strain values measured at both ends of the joint.

Keywords RC interior beam-column joint, Penetrated beam rebar, Column axial load ratio, Bond characteristics, Bond strength, Yield strength of beam rebar

Journal information: ISSN 1976-0485 / eISSN 2234-1315.

*Correspondence:
Kil-Hee Kim
kimkh@kongju.ac.kr
Full list of author information is available at the end of the article

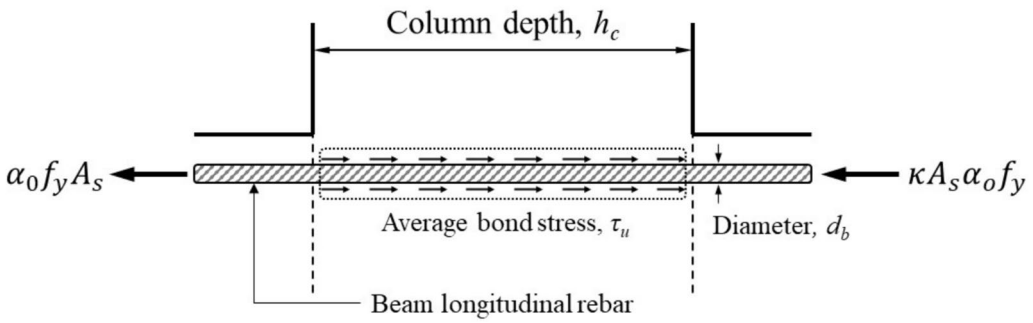

Fig. 1 Forces acting on beam longitudinal rebar penetrating an interior joint panel

1 Introduction and Background

The stability and seismic performance of reinforced concrete (hereafter, RC) structures under seismic loading is highly dependent on how the various elements of the structure interact. In particular, RC moment-resisting frames are widely used as structural systems that play an important role in the absorption and dissipation of seismic energy (Gul et al., 2024). In RC moment resisting frames, if the beam-column joints are not properly designed, the seismic performance can be degraded. In addition, due to joint failure, the columns reduce their capacity to resist celebrations, which can reduce the stiffness of the structure (Pantelides et al., 2017). Two failure modes are considered for RC interior beam-column joints: shear and bond failure. Although there are various opinions on the design of beam-column joints, the general consensus emphasizes the risk of shear failure at the joints. This is because shear failure is brittle and has the potential to reduce the axial bearing capacity of the column (Saghafi et al., 2019). However, the stiffness and energy dissipation history of the beam-column joint is significantly reduced due to bond failure, which is caused by the slippage of the beam longitudinal rebar through the joint (Kitayama et al., 1987). Furthermore, damage caused by bond failure is difficult to detect, and even when detected, it is difficult and expensive to repair(ref). It has also been emphasized that bond failure can reduce the ductility capacity of the beam adjacent to the joint (Hakuto et at., 1999).

As shown in Fig. 1, the beam longitudinal rebar in interior beam-column joints typically relies on the bond force between the concrete and the straight length of the reinforcement through the joint core region (hereafter, column depth h_c) (Brooke et al., 2013). In interior beam-column joints subjected to cyclic loading, sufficient bond length is required because the beam longitudinal rebar is subjected to compressive forces on one side of the joint and tensile forces on the opposite side. Figure 1 is used as a basis for design criteria for beam longitudinal rebar bond at interior beam-column joints. It is assumed that the magnitude of the tensile stress is equal to the yield strength considering the overstrength factor (α_o) of the reinforcement, and the magnitude of the compressive stress is expected to be less than the yield strength of the reinforcement. The rebar must be kept in equilibrium, and the equilibrium force is generated by the bond stresses along the length of the rebar through the joint.

The distribution of these bond stresses is complex, but for design purposes it is assumed that an average bond stress (τ_u) acts along the entire length of the bar at the joint. Subject to the condition of force equilibrium, the bond failure can be expressed as Eq. (1), where Eq. (1) is the ratio of the diameter (d_b) of the rebar through the joint to the depth (h_c) of the column cross-section, which is equal to Eq. (2).

$$\pi d_b h_c \alpha_p \tau_u \geq \frac{\pi d_b^2}{4} \alpha_0 f_y (1+\kappa) \tag{1}$$

$$\frac{d_b}{h_c} \leq \frac{4\tau_u}{\alpha_o f_y (1+\kappa)} \alpha_p \tag{2}$$

where, d_b = the bar diameter of the beam longitudinal reinforcement, h_c = the column depth, τ_u = the average bond stress available over the column depth, α_p = a variable included to account for the influence of column axial compression on bond strength, α_o and f_y = the overstrength factor and yield strength of the beam longitudinal reinforcement, respectively, κ = ratio of compressive stress to tensile stress in beam longitudinal rebar at joint faces.

As shown in column 2 of Table 1, the average bond stress (τ_u) in the design criteria of various countries is expressed as a function of concrete compressive strength, which is an important influencing factor when determining the required column depth of the joint. Jo et al. (this author's Part I paper) directly investigated the influence of concrete compressive

Table 1 Comparison of existing design equations for required column depth

Design criteria	Basic average bond stress (τ_u)	Factor for column axial stress on bond (α_p)	Factor for rebar stresses at joint faces ($\alpha_s = 1 + \kappa$)	Required column depth ($h_{c,\,req}$)
ACI 318-19	–	–	–	$\frac{h_{c,req}}{d_b} \geq 20, \left(atf_y \leq 400\text{MPa}\right)$ $\frac{h_{c,req}}{d_b} \geq 25, \left(atf_y > 400\text{MPa}\right)$
AIJ (2010)	$0.7f'^{\frac{2}{3}}_c$	$1 + \frac{N}{A_g f'_c}$	$1 + \frac{A_s}{A_{s.top}}$	$\frac{d_b}{h_{c,req}} \leq \frac{2.8}{1+\gamma}\left(1 + \frac{f_0}{f'_c}\right)\frac{f'^{\frac{2}{3}}_c}{f_{yu}}$
NCREE-19-001	–	–	–	$\text{Max}\left(h_{c,\text{req}} = \frac{\alpha_0 f_y}{4\sqrt{f'_c}} d_b, 20d_b\right)$
NZS3101 (2006)	$1.5\sqrt{f_c'}$	$0.95 + 0.5\frac{N}{A_g f'_c}$ $(1.0 \leq \alpha_p \leq 1.25)$	$2.55 - \frac{A_s}{A_{s.top}} \leq 1.8$	$\frac{d_b}{h_{c,req}} \leq 6\left(\frac{\alpha_t \alpha_p}{\alpha_s}\right)\alpha_f \alpha_d \frac{\sqrt{f_c'}}{1.25 f_y}$

Note A_s = area of bar group, $A_{s.top}$ = area of bottom beam bars, d_b = diameter of beam longitudinal rebar, f_y = yield strength of beam longitudinal rebar, f'_c = concrete compressive strength, γ = beam reinforcement ratio, f_0 = compressive stress of column (N/A_g), f_{yu} = ultimate strength of beam longitudinal rebar, α_0 = bar overstrength factor, $\alpha_f = 0.85$ for bi-directional loading, $\alpha_t = 0.85$ for a top beam bar in which more than 300 mm of fresh concrete was cast below the bar, $\alpha_t = 1.0$ for all other cases, α_d = facto related to beam plastic regions

strength on the bond characteristics of beam longitudinal rebar through a bond test that directly simulates the stress state inside the joint. Based on the experimental results, the bond failure was classified, and the regression analysis showed that the average bond stress was proportional to three-quarters power of the concrete compressive strength, which is different from the current design standards (AIJ, NZS). However, as shown in Eq. (2), the required bond length ($h_{c,\text{req}}$) of the RC interior beam-column connection is not only influenced by the concrete compressive strength, but also by the column axial force ratio (α_p), yield strength (f_y) and diameter (d_b) of the beam longitudinal rebar. Current design criteria for these influencing factors vary from country to country and may not take into account these factors. The mechanism of bond failure of beam longitudinal rebar at interior beam-column joints is complex and many influencing factors must be considered.

2 Research Significance

In this study, an experimental study was conducted to evaluate the bond characteristics of beam longitudinal rebar penetrated interior beam-column joints and the required column depth. In addition to the concrete compressive strength identified in Part I (Jo et al., 2025), the effects of the column axial force ratio, yield strength of beam longitudinal rebar, and diameter on the joint bond strength were evaluated. In addition, referring to the method presented in Part I (bond failure mechanism, failure mode, etc.), the factors affecting the bond strength and the required column depth were proposed by considering the bond characteristics focused on the column axial force ratio and yield strength of beam reinforcement.

3 Experimental Investigation

The test specimen concept (simulation of stress state of interior beam-column joint) and experimental method (loading method, measurement method) applied in this study were the same as in Part I (Jo et al., 2025). The width of the column (B_c) was designed to be the same as the beam width (B_b) corresponding to one penetrated rebar, and a total of 14 specimens were manufactured by classifying the specimens into S, M, L, and X series based on the depth of the column (h_c, bond length). Table 2 shows the list of specimens. The specimens were **classified** into S-series ($h_c = 400$ mm), M-series ($h_c = 500$ mm), L series ($h_c = 600$ mm), and X series ($h_c = 750$ mm) based on the column depth (h_c). Specimens 10, 15, and 20 of the S and X series had axial load ratio ($N/A_g f'_c = 10\%$, 15%, and 20%) as a detailed variable; the yield strength of the longitudinal rebar of the beams was the detailed variable for the S-600, M-400, 600, and L-400, 600 specimens. Additionally, specimens 19, 25, and 29 of the L series had the diameter of the longitudinal rebar of the beams ($d_b = 19$, 25, and 29 mm) as detailed variable. The concrete was cast with the column side (column depth direction) facing upward; the same batch of ready-mixed concrete was used for each. Concrete cylinders were manufactured at the same time as the pouring, and compressive strength tests (ASTM, 2021) were conducted before and after the experiment. The average values are shown in the second column of Table 2. The reinforcing bars applied to the reinforcement were subjected to tensile tests; the results are shown in the third, sixth, and eighth columns of Table 2. Meanwhile, the yield strengths (f_y) of SD400 and SD600 of D19, the longitudinal rebar of the beam, were 439 MPa and 628 MPa, respectively, and the yield strains (ε_y) were 2400 με and 4100 με, respectively.

Table 2 Specifications of specimens

Speci-mens	f'_c(MPa)	Beam			Column					$\frac{N}{A_g f'_c}$
		Longitudinal rebars		Section (mm × mm)	Longitudinal rebars		Hoop rebars		Section (mm × mm)	
		f_{by} (MPa)	n_b		f_{cy} (MPa)	n_c	f_{hy} (MPa)	n_h		
S-10	27.9	439	1-D19	150×150	426	8-D19	457	D10@75	400×150	0.10
S-15	27.9	439	1-D19	150×150	426	8-D19	457	D10@75	400×150	0.15
S-20	27.9	439	1-D19	150×150	426	8-D19	457	D10@75	400×150	0.20
S-600	51.0	628	1-D19	150×150	426	8-D19	457	D10@75	400×150	0.10
M-400	51.0	439	1-D19	150×150	426	8-D19	457	D10@75	500×150	0.10
M-600	51.0	628	1-D19	150×150	426	8-D19	457	D10@75	500×150	0.10
L-400	27.9	439	1-D25	150×150	426	8-D19	457	D10@75	600×150	0.10
L-600	27.9	628	1-D19	150×150	426	8-D19	457	D10@75	600×150	0.10
L-19	25.1	439	1-D19	150×150	426	8-D19	457	D10@75	600×150	0.10
L-25	25.1	439	1-D25	150×150	426	8-D19	457	D10@75	600×150	0.10
L-29	25.1	439	1-D29	150×150	426	8-D19	457	D10@75	600×150	0.10
X-10	27.9	628	1-D29	150×150	426	8-D19	457	D10@75	750×150	0.10
X-15	27.9	628	1-D29	150×150	426	8-D19	457	D10@75	750×150	0.15
X-20	27.9	628	1-D29	150×150	426	8-D19	457	D10@75	750×150	0.20

Note f_{by} = yield strength of longitudinal rebar of beam, n_b = size of longitudinal rebar in beam, f_{cy} = yield strength of longitudinal rebars of column, n_c = size of longitudinal rebars in column, f_{hy} = yield strength of hoop rebar in column, n_h = size of hoop bar, $N/(A_g f'_c)$ = Axial load ratio of column

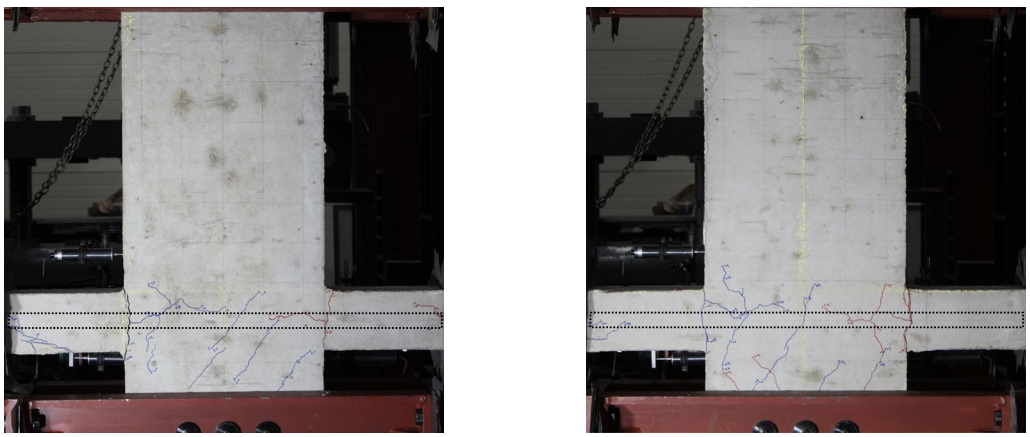

(a) M-400 (b) M-600

Fig. 2 Comparison of representative crack patterns at failure

4 Experimental Results

4.1 Crack Patterns and τ-Slip Relationship

Figure 2 shows the crack patterns of the M-400 and M-600 specimens. Due to the thickness of the cover that surrounds the beam longitudinal rebar, no cracks on the surface were observed; however, the bond characteristics of the beam longitudinal rebar can be measured using WSG and LVDT. No cracks were found in the upper part of the column in any of the specimens. The cracks shown in blue in the figure are part of the distribution of cracks that occurred in the positive direction; red represents the distribution of cracks in the negative direction. In the early stage of loading ($0.25\varepsilon_y$), vertical cracks occurred in the concrete blocks near the column boundary for both the M-400 and M-600 specimens. Afterwards, as the load increased, cracks progressed from the tensile side to the compression side along the beam longitudinal rebar (solid line) in both positive and negative directions.

In addition, to compare the bond characteristics of each test specimen, the relationship between the bond stress (τ) and the slip amount (Slip) is shown in Fig. 3. The relationship between bond stress and slip was checked by

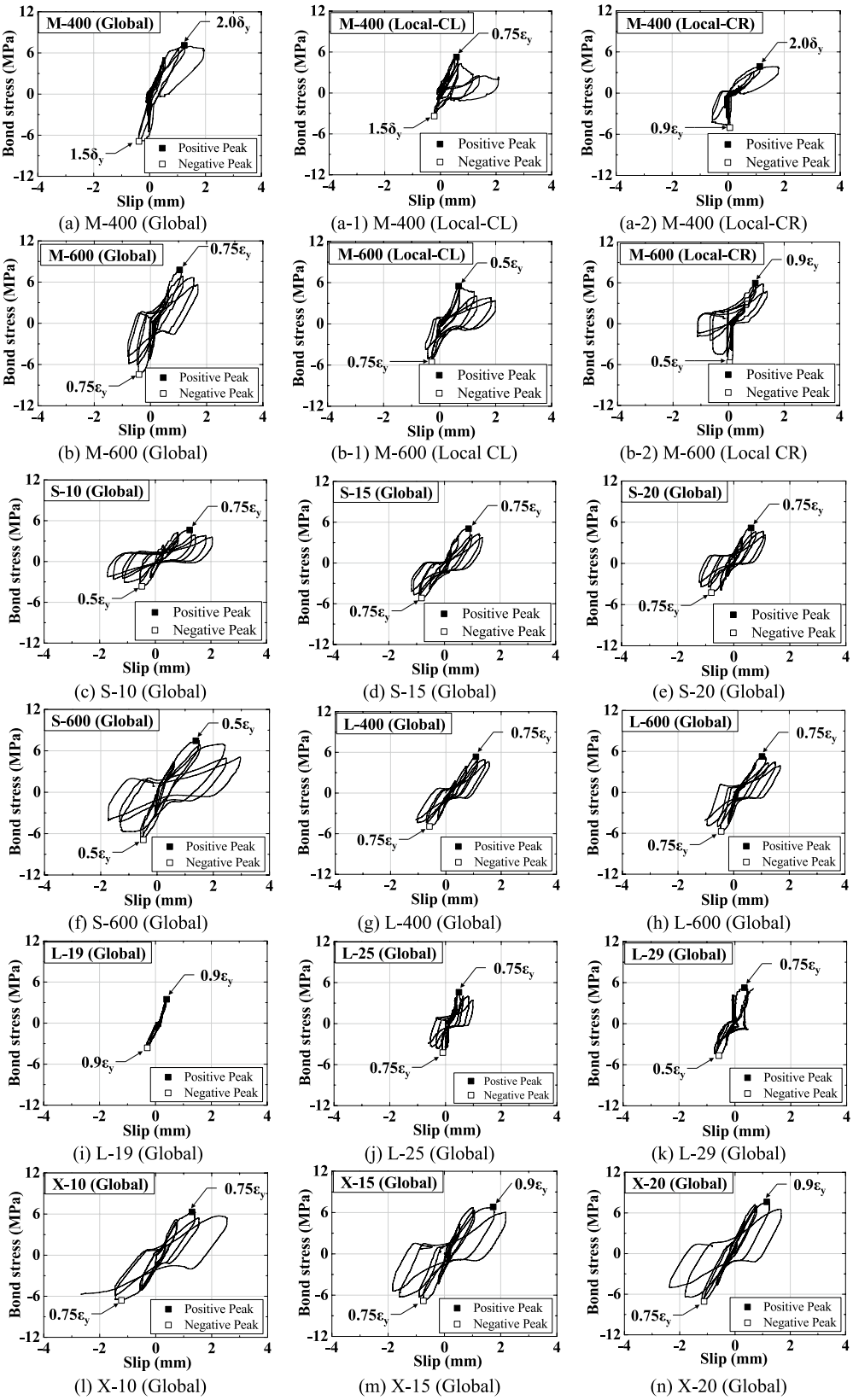

Fig. 3 Bond stress-slip relationship

Table 3 Amount of bond stress and slippage at peak for each region (positive direction)

Specimens	Local CL			Local CR			Global		
	peak (ε_y)	τ_{CL} (MPa)	S_{CL} (mm)	Peak (ε_y)	τ_{CR} (MPa)	S_{CR} (mm)	Peak (ε_y)	τ_{Global} (MPa)	S_{Global} (mm)
S-10	0.50	5.75	0.82	0.75	8.83	1.19	0.75	4.59	1.24
S-15	0.50	4.87	0.52	0.75	5.13	0.74	0.75	5.01	0.86
S-20	0.50	3.29	0.38	0.90	5.35	0.98	0.75	5.16	0.60
S-600	0.25	4.36	0.61	0.50	5.49	1.27	0.50	7.43	1.44
M-400	0.75	5.12	0.49	2.00	3.78	1.78	1.50	6.62	0.98
M-600	0.50	5.50	0.68	0.90	5.83	1.23	0.75	7.76	1.00
L-400	0.75	2.24	1.18	0.90	4.54	1.27	0.75	5.34	1.07
L-600	0.90	3.48	1.74	0.75	2.79	0.91	0.75	5.23	1.08
L-19	0.90	3.86	0.30	0.90	1.96	0.49	0.90	3.48	0.38
L-25	0.75	2.76	1.34	0.90	3.89	1.43	0.75	4.59	0.47
L-29	0.90	4.08	1.40	0.90	3.06	1.06	0.75	5.25	1.66
X-10	0.50	2.72	0.90	0.75	4.61	1.14	0.75	6.31	1.28
X-15	0.50	4.93	0.64	0.90	7.79	1.56	0.90	6.76	1.73
X-20	0.75	5.73	0.84	0.90	5.48	1.10	0.90	7.61	1.21

dividing the section centering on the joint panel zone. As confirmed by the crack pattern, the LVDT L and R and the strain gauges J1 and J6 were excluded due to the influence of vertical cracks that occurred in the concrete block located at the column boundary in the initial stage of loading. The bond stress and slip amount in the figure were calculated using the values measured by the WSG and LVDTs attached to the beam longitudinal rebar, as shown in Eqs. (3) and (4) (see Jo et al., 2025). In Eq. (4), $\text{Slip}_{\text{LVDT}}$ represents the slip value of the longitudinal reinforcement, and $\text{Slip}_{\text{LVDT}}$ represents the value excluding the length, which increased due to deformation of the longitudinal reinforcement.

$$\tau = \frac{(\varepsilon_{s1} + \varepsilon_{s2})A_{st}E_s}{\psi l_s} \tag{3}$$

$$\text{SLIP} = \text{Slip}_{\text{LVDT}} - l_s(\varepsilon_{s1} - \varepsilon_{s2}) \tag{4}$$

Here, ε_{s1}, ε_{s2} = longitudinal reinforcement strain of test area for bond stress measurement; A_{st} = area of longitudinal reinforcement; E_s = elastic modulus of longitudinal reinforcement; ψ = nominal circumference of longitudinal reinforcement; l_s = length from ε_{s1} to ε_{s2}.

As described in Part I paper Section 3.2, to check the bond characteristics in the core region of the joint in detail, the SLIP is divided into Local CL and Local CR, and the corresponding bond stresses are the bond stresses calculated in zone 1 and zone 3 (Jo et al. 2025). The SLIP in the global section was calculated using the average value of LVDT CL and CR. The WSG J2 ~ J5 section was defined as the joint core region (Global) in the joint panel area where the beam longitudinal rebar had penetrated (Jo et al.). The local area was defined as the area subjected to tension and compression under cyclic loading in the joint core area based on LVDT CL and CR.

Figure 3a, a-1, a-2, and Table 3 show the relationship between the bond stress and slip for each section of the M-400 specimen. In the local CL, the maximum bond stress was reached at $0.75\varepsilon_y$ during positive direction loading and then decreased in subsequent cycles. On the other hand, the Local CR showed a healthy state without any decrease in bond stress even after the $0.90\varepsilon_y$ yield cycle. In the global area, the longitudinal rebar showed a healthy state without decrease in the bond stress before yielding; there was no pinching phenomenon because an increase in slip amount was observed. This phenomenon was also observed in the L-19 and X-20 specimens, as shown in Fig. 3i, n.

On the other hand, the bond stress-slip relationship of the M-600 specimen in Fig. 3b, b-1, b-2, which used high-strength reinforcing bars for beam longitudinal rebar, showed a trend different from that of the M-400 specimen, which used normal-strength reinforcing bars. As shown in Fig. 3b-1, the bond stress of the local CL reached the maximum bond stress (5.50 MPa) at $0.50\varepsilon_y$ during positive direction loading; then, the bond stress decreased at the next cycle of $0.75\varepsilon_y$. The bond stress in the local-CR area reached the maximum bond stress (5.83 MPa) at $0.90\varepsilon_y$, and the bond stress in the global area reached the maximum point in the previous cycle ($0.75\varepsilon_y$). After that, the bond stress decreased in the yield cycle ($0.90\varepsilon_y$). Based on the results of these experiments, the bond stress in the core region of the joint first

disappeared in the tensile region (Local CL), and then transferred to the compressive region (Local CR); the burden of the bond stress thus increased. Finally, the core region (global) of the joint was relieved of bond stress due to the loss of bond stress in the compression region. This phenomenon was also observed in the negative direction; however, the maximum bond stress was reached in the low load cycle due to the influence of the preceding positive direction load.

The amount of slippage increased significantly after the maximum bond stress was reached in each section, showing a pinching phenomenon that was seen in previous studies (Kitayama et al., 1987). The reason for this is that the application of high-strength rebar to the beam longitudinal rebar increased the internal bond stress at the joint; however, the same column depth was applied as for the M-400 specimen. This phenomenon was observed in the S-10, 15, and 20, and the S-600, L-400, 600, L-25, L-29, and X-10 and 15 specimens in the same manner as shown in Fig. 3c–m.

4.2 Strain and Bond Stress Distribution of Beam Longitudinal Rebar

The strain distribution of longitudinal reinforcing bars under positive direction of loading is shown in Fig. 4. The strain distribution showed the strain corresponding to the first cycle of each loading cycle in the panel area of the joint. In general, at the initial stage of loading ($0.25\varepsilon_y$), all specimens showed a strain distribution in the form of a constant slope from the tensile side (J1) to the compression side (J6). After that, differences between test subjects were seen as the number of cycles increased. As shown in Fig. 4f, the M-600 specimen showed a larger increase in the strain rate of J2 than that of J3 in the $0.50\varepsilon_y$ cyclic loading; it then showed the opposite strain rate increase in $0.75\varepsilon_y$, resulting in a reversal of slope (bond stress degradation, bond failure) in zone 1. After that, the same slope reversal phenomenon appeared in zone 2 and zone 3 at the time of the $0.90\varepsilon_y$ yield cycle. The same trend was observed in the S-10, 15, 20, and 600 and L-400, 600, 25, and 29, and X-10 and 15 specimens.

In contrast, as shown in Fig. 4e, the M-400 specimen exhibited slope reversal phenomenon due to the difference in the strain increase in zone 1 at the time of the $0.90\varepsilon_y$ cyclic loading, as did the M-600 specimen; however, this phenomenon did not occur in zone 2 or zone 3. The L-19 and X-20 test subjects showed the same trend as the M-400 test subject. The reason for this is explained in Sect. 3.1: the bond deterioration between the rebar and concrete in the core region of the joint gradually progressed from the region near the tensile side to the region near the compression side.

In addition, the distribution of bond stresses, calculated quantitatively, is shown in Fig. 5 and Table 4 to check the change in bond stress in each zone (zones 1, 2, and 3). The bond stress was calculated according to the difference in strain in each area, as shown in Eq. (3). As shown in Fig. 5f, the M-600 specimen exhibited a bond stress of 4.36 MPa at zone 1, which is close to the tensile side, under a $0.25\varepsilon_y$ cyclic load in the core region of the joint. At the same time, the bond stresses in zone 2, the central part of the core region, and zone 3, which is close to the compression side, were 6.24 and 1.82 MPa. After that, the bond stress in zone 1 decreased to a low level of 3.61 MPa at $0.5\varepsilon_y$, but zone 2 showed a high increase of 12.2 MPa. At $0.75\varepsilon_y$, the **bond stress** in zone 1 was 3.68 MPa, which was lower than that of the previous load cycle, but the bond stress in zone 2 increased to 11.8 MPa. At $0.9\varepsilon_y$, which is just before yielding of the longitudinal reinforcing bars, the bond stress in zone 2 was 8.41 MPa, which was lower than that of the previous load cycle.

In contrast, the M-400 specimen showed the same trend as the M-600 specimen at $0.25\varepsilon_y$, with values of 1.24 MPa in zone 1 and 0.81 and 0.09 MPa in zones 2 and 3, respectively, which are about 65% and 7% lower, respectively. Then, at $0.5\varepsilon_y$, the **bond stresses** in zone 1 and zone 2 increased significantly to 3.24 and 2.55 MPa, respectively; however, the **bond stress** in zone 3 increased less. At $0.9\varepsilon_y$, when the bond stress decreased after the maximum bond stress of zone 1 was reached, zone 2 saw a large increase of 7.71 MPa, and the bond stress of zone 3 saw a small increase of 0.87 MPa. The bond stresses in zones 2 and 3 did not decrease in subsequent load cycles. Based on these experimental results, this study concluded that the bond stress in zone 2, which is the center of the joint core region before yielding of the beam longitudinal rebar, decreased after reaching the maximum bond stress. The 14th column of Table 4 shows the bond failure status of all experimental specimens.

5 Parametric Assessment for Required Column depth of Interior Joints

5.1 Effect of Column Axial Load Ratio

As explained in Chapter 1, the required column depth ($h_{c.\mathrm{req}}$) in the existing concrete design criteria shown in Table 1 is presented in various ways, such as simply defining it based on the yield strength of the longitudinal rebar of the beam or defining it under the assumption that the bond strength (τ_u) is greater than the bond stress (τ_f) caused by flexural moments, as in Eq. (1). The bond stress suggested in the existing criteria, AIJ (2010) and NZS 3101 (2006), considers the effects of the column axial load ratio as well as the concrete compressive strength; however, AC 318-19 and NCREE-19-001 do not take it into account. To evaluate the suitability of

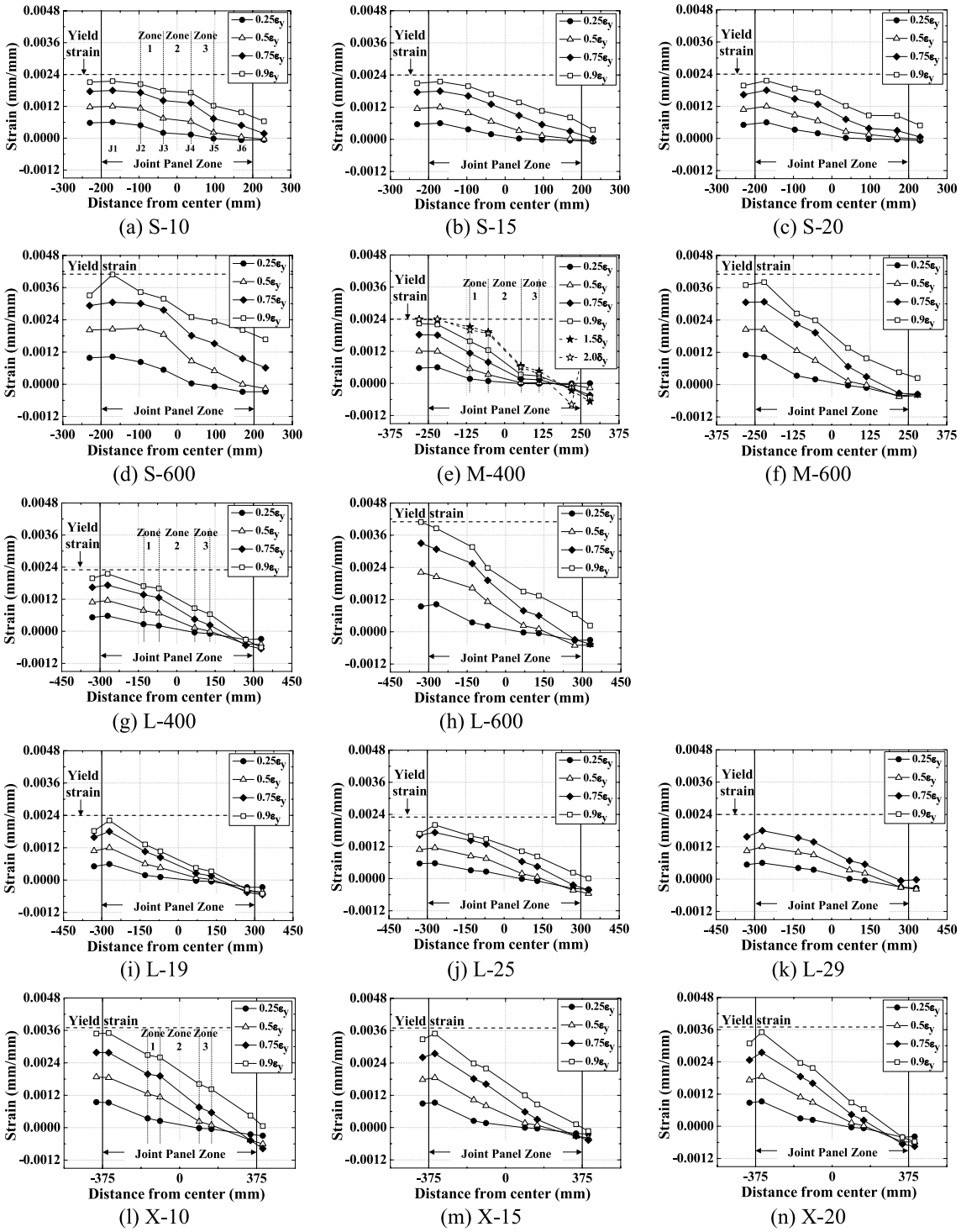

Fig. 4 Strain distribution of beam longitudinal rebar in joint panel zone (positive direction)

the required column depth suggested in the existing criteria, the required column depth ratio ($h_c/h_{c.\mathrm{req}}$) according to the column axial load ratio ($N/A_g\ f'_c$) is shown in Fig. 6. Here, h_c refers to the column depth applied to the experiment in this study, and $h_{c.\mathrm{req}}$ refers to the required column depth suggested by the existing criteria. If $h_c/h_{c.\mathrm{req}}$ is greater than 1, it is judged as a "Secure bond"; if it is less than 1, it is judged as "Bond failure". The

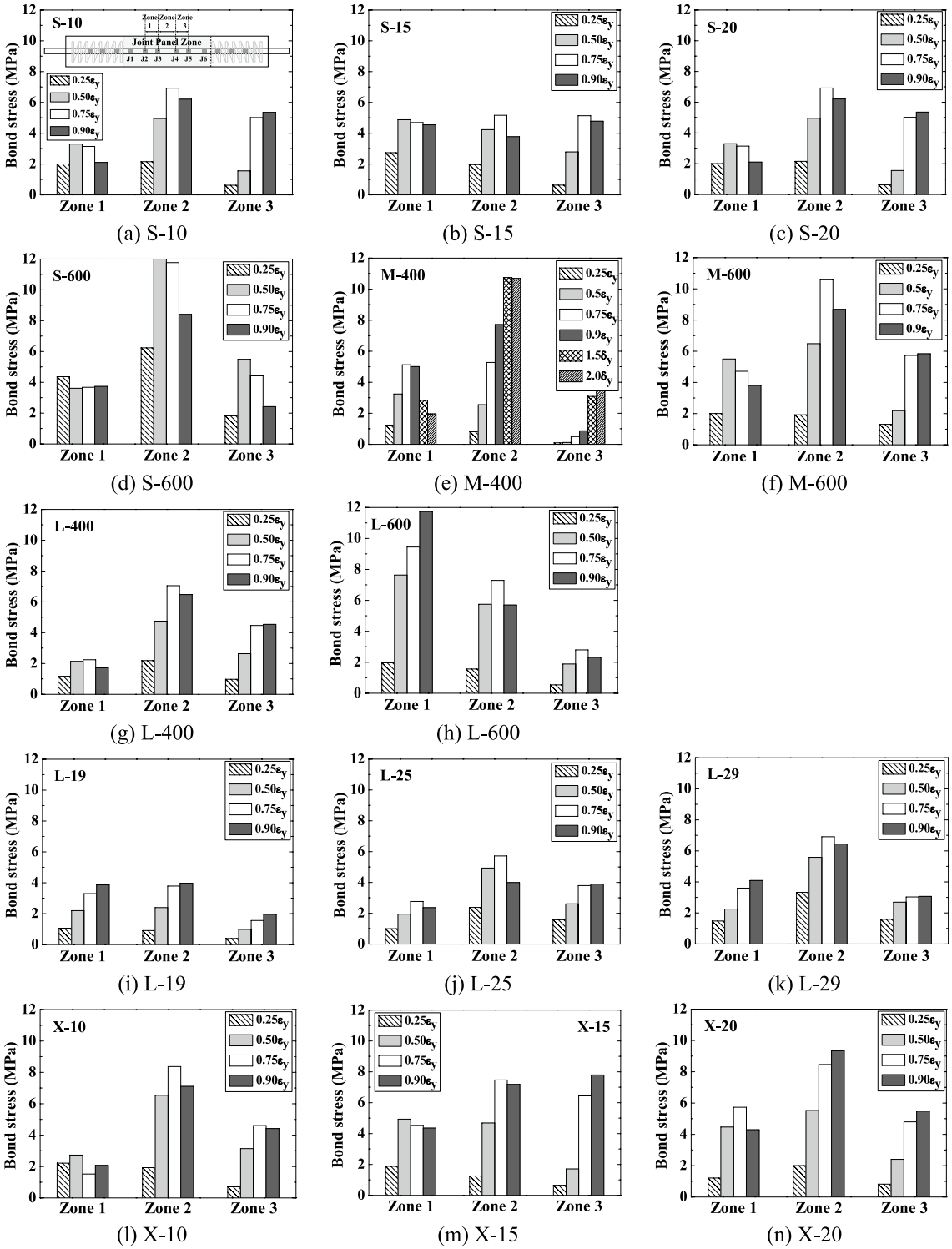

Fig. 5 Bond stress distribution each zone (positive direction)

experimental results were applied as failure type based on whether there was bond failure, as determined in Sect. 3.2.

As shown in Fig. 6a, c, the American ACI 318-19 and Taiwan's NCREE 19-001 standards do not reflect the influence of the column axial load ratio, so they show a

Table 4 Bond stress for each region (positive direction)

Speci-mens	Bond stress (MPa)												Failure mode
	$0.25\varepsilon_y$			$0.50\varepsilon_y$			$0.75\varepsilon_y$			$0.90\varepsilon_y$			
	Zone1	Zone2	Zone3	Zone1	Zone2	Zone3	Zone1	Zone2	Zone3	Zone1	Zone2	Zone3	
S-10	4.29	0.78	2.31	5.76	1.51	6.16	4.50	1.20	8.83	3.76	0.85	7.50	Bond failure
S-15	2.73	1.96	0.63	4.87	4.23	2.78	4.69	5.16	5.13	4.55	3.77	4.78	Bond failure
S-20	2.00	2.15	0.62	3.29	4.95	1.55	3.14	6.92	5.02	2.10	6.21	5.35	Bond failure
S-600	4.36	6.24	1.82	3.61	12.2	5.49	3.68	11.8	4.41	3.73	8.41	2.42	Bond failure
M-400	1.24	0.81	0.09	3.24	2.55	0.12	5.13	5.27	0.49	5.01	7.71	0.87	Secure bond
M-600	2.00	1.92	1.31	5.50	6.48	2.19	4.71	10.6	5.73	3.80	8.68	5.83	Bond failure
L-400	1.17	2.18	0.97	2.14	4.75	2.64	2.24	7.05	4.47	1.71	6.48	4.54	Bond failure
L-600	1.40	1.56	0.54	2.42	5.74	1.88	2.87	7.29	2.79	3.48	5.69	2.32	Bond failure
L-19	1.06	0.90	0.39	2.19	2.39	0.98	3.29	3.78	1.55	3.86	3.97	1.96	Secure bond
L-25	0.99	2.38	1.58	1.94	4.93	2.61	2.76	5.72	3.79	2.36	3.99	3.89	Bond failure
L-29	1.48	3.32	1.59	2.25	5.59	2.69	3.59	6.91	3.03	4.08	6.44	3.06	Bond failure
X-10	2.22	1.93	0.71	2.72	6.53	3.14	1.52	8.37	4.61	2.07	7.11	4.42	Bond failure
X-15	1.87	1.25	0.65	4.93	4.69	1.71	4.53	7.47	6.44	4.35	7.19	7.79	Bond failure
X-20	1.21	2.01	0.82	4.46	5.52	2.40	5.73	8.46	4.80	4.29	9.33	5.48	Secure bond

constant required column depth ratio and do not properly predict the experimental results. The Japanese AIJ (2010) and New Zealand's NZS 3101 (2006) standards predict more accurately than do the other standards; however, it was confirmed that the suitability is poor at high axial load ratios (Fig. 6b, d). These analysis results show that the required bond length of the beam longitudinal rebar penetrating the interior beam-column joint is affected by the axial load ratio and needs to be considered in the bond strength equation.

Regression analysis was performed to reflect the influence of the column axial load ratio by applying the data of Fujii et al. (1991), which was obtained in an experiment similar to the experiment performed in this study, as shown in Fig. 7c.

The experimental data applied to the regression analysis also included the "secure bond" specimens. In addition, the data were expressed as Eq. (5) to exclude other influencing factors such as the compressive strength of concrete, the yield strength of reinforcing bars, and the diameter.

$$\text{Bond stress increase ratio}(\%) = \tau_{u.15\%,20\%} < \tau_{u.10\%} \tag{5}$$

As the axial load ratio of the column increased, the peak bond stress at the joint tended to increase linearly. Reflecting this tendency, the regression analysis showed that the maximum bond stress increased with the axial load ratio by a factor of about 1.13. Reflecting this trend, the influence factor (α_p) of the axial load ratio of the column is proposed in Eq. (6). Here, the range of column axial force ratio was determined by referring to the existing study (Park et al., 1988) that the bond characteristics of the joint are not significantly affected when the α_p is less than 1.0.

$$\alpha_p = \left(0.89 + 1.11\frac{N}{A_g f'_c}\right)(1.0 \le \alpha_p) \tag{6}$$

where N is the compressive load applied to the column (kN), A_g is the area of the column (mm^2), and f'_c is the compressive strength of concrete (MPa). To evaluate the validity of the proposed equation, it is compared with αp, given by the current design criteria (Fig. 7a, b). As shown in Fig. 7a, the Japanese AIJ (2010) standard overestimates the experimental results, with a coefficient of variation of 33.9%, which is higher than that of the proposed formula. As shown in Fig. 7b, the NZS 3101 (2006) standard from New Zealand tends to be conservative, underestimating the experimental results. It also shows poor fit, with a coefficient of variation of 53.6%. As shown in Fig. 7c, the coefficient of variation of the proposed equation is 30.7%, which is a good prediction compared to the current design equation.

5.2 Effect of Beam Flexural Rebar Yield Strength and Diameter

The bond stress distribution for each loading cycle is shown in Fig. 8 for the specimen with the yield strength and diameter of the beam longitudinal rebar through the

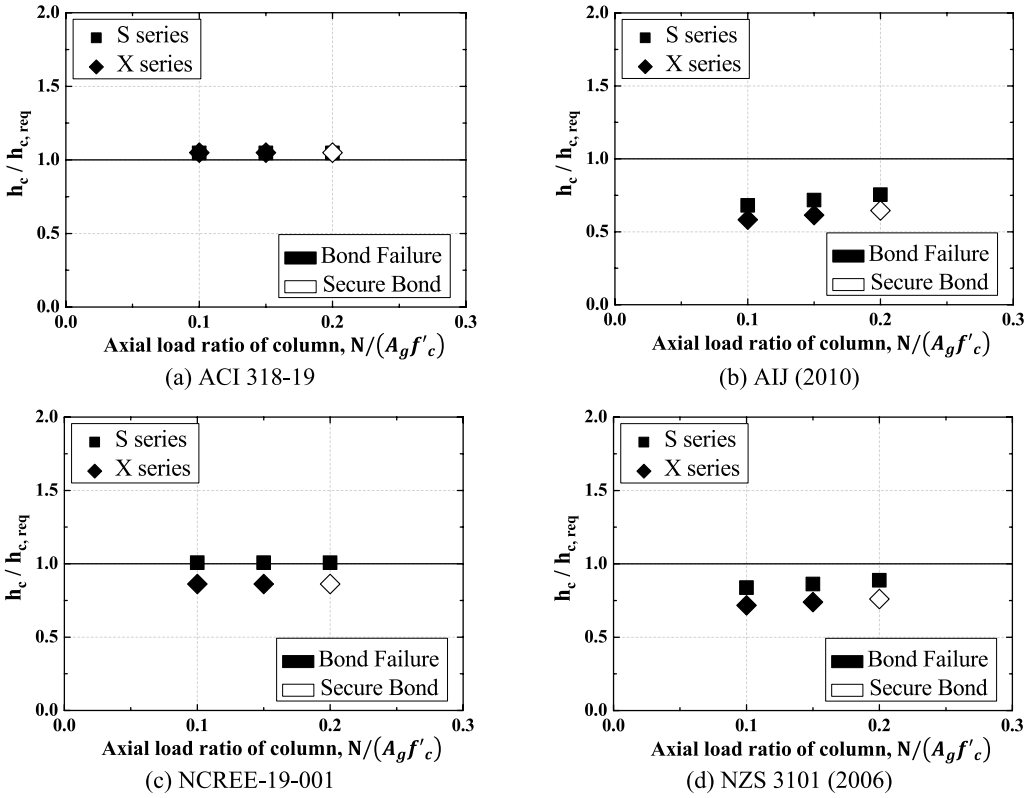

Fig. 6 Relationship of Axial load ratio ($N/A_g f'_c$) and required column depth ratio ($h_c/h_{c,req}$)

joint as variables. It is shown in Fig. 8a that when high strength (f_y = 600 MPa) rebar is applied to the beam longitudinal rebar, the increase in the bond stress is significantly increased compared to the normal strength (f_y = 400 MPa) rebar. Due to this effect, when the same column depth is applied, the M-600 specimen with high-strength rebar is at risk of bond failure because the required column depth is shorter than the M-400 specimen; the actual experimental results showed bond failure. The same phenomenon was also observed in the specimen with the diameter of beam longitudinal rebar as a variable, as shown in Fig. 8b. Table 1 shows that existing criteria vary the required column depth to reflect the influence of beam longitudinal rebar on the yield strength. To evaluate the appropriateness of the required column depths in the existing criteria, the ratio ($h_c/h_{c.\mathrm{req}}$) of the required column depth to the yield strength of the reinforcement is shown in Fig. 9. Here, h_c refers to the column depth applied to the experiments in this study, and $h_{c.\mathrm{req}}$ refers to the required column depth proposed by the existing criteria.

If $h_c/h_{c.\mathrm{req}}$ is greater than 1, it is determined as a "Secure bond;" if it is less than 1, it is determined as "Bond failure". The experimental results were applied to the failure type based on the bond failure determined in Sect. 3.2. As shown in Fig. 8a, c, the failure types of most specimens are not properly predicted by the ACI 318-19 of the American standards or by NCREE-19-001 of Taiwan. The NZS 3101 (2006) of New Zealand predicts the "Secure bond" specimens well but does not properly predict the "Bond failure" specimens. Based on these results, the effect factor was calculated by focusing on the stress difference (Δf_s) at both ends of the main reinforcing bars penetrating the joint. Figure 10 shows the stress at both ends of the joint, which was calculated using the strain values measured on the tensile side (J1) and the compressive side (J6) at the time of reaching maximum bond stress for specimens judged as "Bond failure". Compared to the tensile stress (f_s), the compressive stress (f'_s) was distributed variously from 13 to 43%, and the influencing factor Δf_s, calculated by applying the average value, was expressed as in Eq. (6); the bond stress (τ_f) caused by flexural moment was proposed as in Eq. (7).

$$\Delta f_s = (1 + 0.25) f_y \tag{7}$$

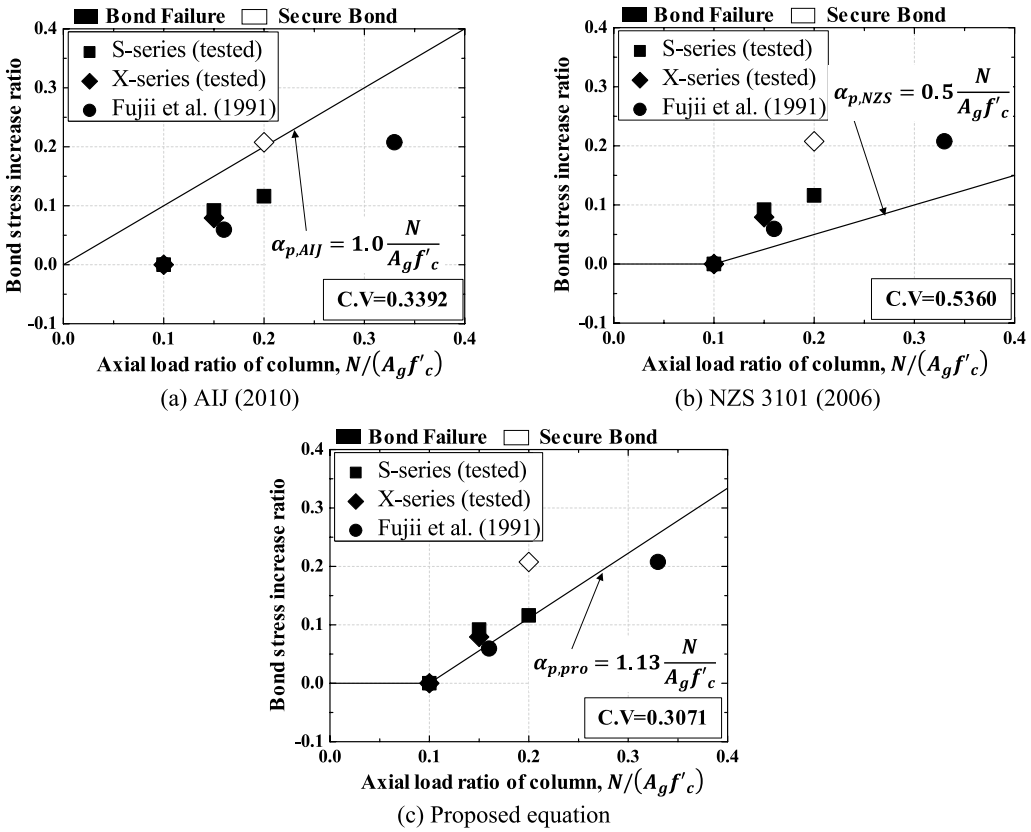

Fig. 7 Comparison of bond strength equation by column axial load ratio

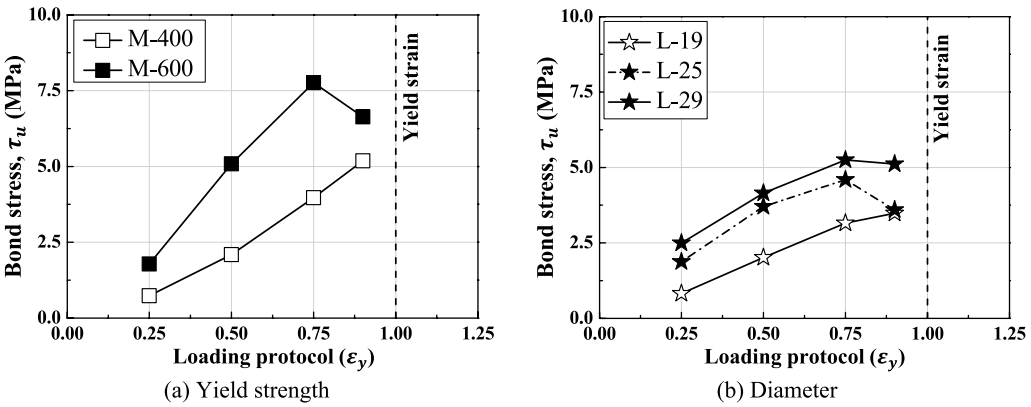

Fig. 8 Effect of yield strength and diameter of beam flexural rebar on maximum bond stress

$$\tau_f = \frac{(1+0.25)f_y d_b}{4h_c} \tag{8}$$

6 Conclusion

This study was conducted to directly investigate the effects of column axial force ratio and beam longitudinal rebar yield strength and diameter on bond characteristics at interior beam-column joints. Through bond stress-slip relationship, beam longitudinal rebar strain, and bond stress distribution, it was confirmed that the same bond failure mechanism as presented in Part I occurred, and the following conclusions were additionally drawn.

(1) The maximum bond stress of the joint tended to increase linearly as the column axial load ratio

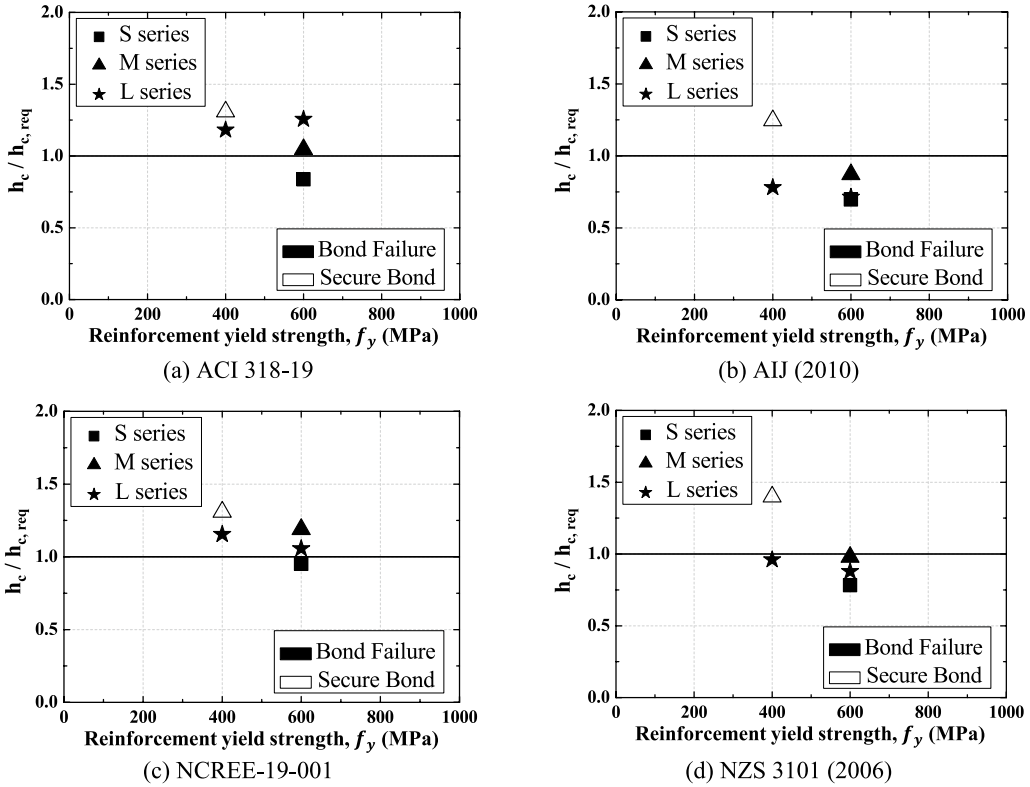

Fig. 9 Relationship of rebar yield strength (f_y) and required column depth ratio ($h_c/h_{c,req}$)

increased; the effect factor (α_p) of the column axial load ratio on the bond strength was proposed based on the experimental results. The proposed equation showed excellent prediction performance compared to the existing criteria equation, with a coefficient of variation of 30.7%.

(2) When high-strength rebar is applied to beam longitudinal rebar, the increase in bond stress is greater than that of normal-strength rebar, and the risk of bond failure was confirmed at the same column depth. In addition, a bond stress (τ_f) equation that reflects the stress difference of the beam longitudinal was proposed using the strain values measured at both ends of the joint.

(3) Through the study of Parts I and II, it was found that the bond characteristics of longitudinal rebar penetrated the interior beam-column joint are affected by various factors such as concrete compressive strength, column axial force ratio, yield strength, and diameter, and further research is needed to calculate the required column depth by combining each influencing factor.

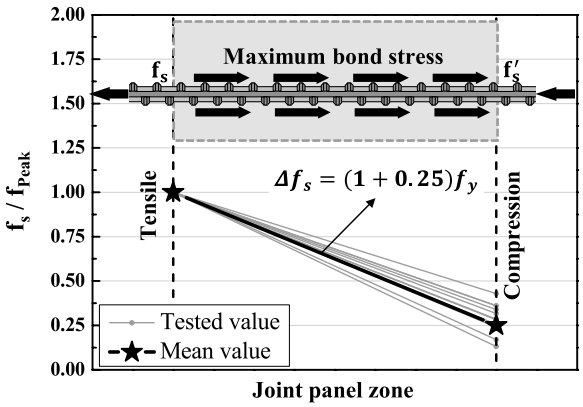

Fig. 10 Factor for beam flexural rebar stresses at both ends of joint

Acknowledgements
Not applicable.

Author contributions
M. Jo: data curation, investigation, project administration, visualization, writing—original draft, H. Kim: conceptualization, methodology, D. Kim: formal analysis, S. Lim: formal analysis, S. Jeong: data curation, J. Lee: methodology, K. Kim: conceptualization, funding acquisition, project administration, supervision, writing—review and editing. All authors have read and agreed to the published version of the manuscript.

Funding
This work was supported by the National Research Foundation of Korea(NRF) grant funded by the Korea government(MSIT) (2023R1A2C3002443); This research was supported by Basic Science Research Program through the National Research Foundation of Korea(NRF) funded by the Ministry of Education (2019R1A6A1A03032988); This research was supported by Basic Science Research Program through the National Research Foundation of Korea(NRF) funded by the Ministry of Education (RS-2023-00239201); This research was supported by Korea Basic Science Institute (National research Facilities and Equipment Center) grant funded by the Ministry of Education (RS-2022-NF000835).

Availability of data and materials
Some or all data, models, or code that support the findings of this study are available from the corresponding author upon reasonable request.

Declarations

Ethics approval and consent to participate
All authors of the manuscript confirm the ethics approval and consent to participate following the Journal's policies.

Consent for publication
All authors of the manuscript agree on the publication of this work in the International Journal of Concrete Structures and Materials.

Competing interests
The authors declare that they have no competing interests.

Author details
[1]Department of Architectural Engineering, Kongju National University, Gongju-si, Republic of Korea. [2]Department of Green Smart Architectural Engineering, Kongju National University, Gongju-si, Republic of Korea. [3]School of Civil, Architectural Engineering and Landscape Architecture, Sungkyunkwan University, Seoul, Republic of Korea. [4]Department of Green Smart Architectural Engineering and Urban Systems Engineering, Kongju National University, Gongju-si, Republic of Korea.

Received: 17 March 2025 Accepted: 29 May 2025
Published online: 24 September 2025

References

ACI (American Concrete Institute). (2019). Building code requirements for structural concrete and commentary, ACI 318-19. Farmington Hills, MI: ACI.
AIJ (Architectural Institute of Japan). (2010). AIJ standard for structural calculation of reinforced concrete structures. Tokyo: AIJ.
ASTM. (2021). Standard test method for compressive strength of cylindrical concrete specimens. ASTM C39/C39M-21. West Conshohochen, PA: ASTM 2021.
Brooke, N. J., Megget, L. M., & Ingham, J. M. (2006) Bond performance of interior beam-column joints with high-strength reinforcement. *ACI Structural Journal, 103*(4), 596–603. https://doi.org/10.14359/16436
Fujii, S., Murakami, H., Yamada, T., & Morita, S. (1991). Bond properties of beam through bars in high-strength reinforced concrete beam-column joints. *Proceedings of the Japan Concrete Institute, 13*(2), 483–488.
Gul, M. A. A., Khan, S. W., Noor, U. A., Khan, F. A., & Khaliq, W. (2024). Comparative study of RC and ECC beam-column connections with shear deficit spacing under quasi-static conditions. *Journal of Structural Integrity and Maintenance, 9*(4), 2435187. https://doi.org/10.1080/24705314.2024.2435187
Hakuto, S., Park, R., & Tanaka, H. (1999). Effect of deterioration of bond of beam bars passing through interior beam-column joints of flexural strength and ductility. *ACI Structural Journal, 96*(5), 858–864. https://doi.org/10.14359/740
Jo, M. S., Kim, H. G., Kim, D. H., Lim, S. A., Choi, Y. S., Lee, J. Y., & Kim K. H. (2025). Proposal for bond strength considering bond characteristics of beam flexural rebar on interior beam-column joints. Part I: Focusing on concrete compressive strength. International Journal of Concrete Structure Materials.
NCREE (2019). Design Guideline for Building of High-Strength Reinforced Concrete Structures (Draft) (NCREE-19-001). Taipei, Taiwan: National Center for Research on Earthquake Engineering.
NZS 3101 (2006). Concrete structures standard part 1-the design of concrete structures, Wellington. Standards New Zealand: New Zealand.
Pantelides, C. P., Hansen, J., Ameli, M. J., & Reaveley, L. D. (2017). Seismic performance of reinforced concrete building exterior joints with substandard details. *Journal of Structural Integrity & Maintenance, 2*(1), 1–11. https://doi.org/10.1080/24705314.2017.1280589
Park, R., & Ruitong, D. (1988). A comparison of the behaviour of reinforced concrete beam-column joints designed for ductility and limited ductility. *Bulletin of the New Zealand National Society for Earthquake Engineering, 21*(4), 255–278. https://doi.org/10.5459/bnzsee.21.4.255-278
Saghafi, M. H., Shariatmadar, H., & Kheyroddin, A. (2019). Seismic behavior of high-performance fiber-reinforced cement composites beam-column connection with high damage tolerance. *Int. J. Concr. Struct. Mater, 13*, 14. https://doi.org/10.1186/s40069-019-0334-3

Publisher's Note

Min-Su Jo Research Assistant Professor, Department of Architectural Engineering, Kongju National University, Republic of Korea.

Hyeong-Gook Kim Associate Professor, Department of Green Smart Architectural Engineering, Kongju National University, Republic of Korea.

Dong-Hwan Kim Research Assistant Professor, Department of Architectural Engineering, Kongju National University, Republic of Korea.

Su-A Lim Research Assistant Professor, Department of Architectural Engineering, Kongju National University, Republic of Korea.

Si-Hyeon Jeong Staff, Division of Structural Business, J. Tec Structural Engineering, Republic of Korea.

Jung-Yoon Lee Professor, School of Civil, Architectural Engineering and Landscape Architecture Sungkyunkwan University, Republic of Korea.

Kil-Hee Kim Professor, Department of Green Smart Architectural Engineering & Urban Systems Engineering, Kongju National University, Republic of Korea.